*Acta Cryst.* (1988). A44, 1036-1042

# The Shapes of Single-Crystal Neutron Reflections in Relation to their Experimental Components

BY A. MCL. MATHIESON

*Chemistry Department, La Trobe University, Bundoora, Victoria, Australia* 3083

(*Received* 18 *January* 1988; *accepted* 6 *June* 1988)

## Abstract

The shapes of Bragg reflections in $\Delta\omega, \Delta 2\theta$ space, resulting from the diffraction of monochromated neutrons from a small single crystal, *c*, are related, by means of a graphical or diagram approach rather than the more usual analytical treatment, to the various components of the experimental arrangement, namely an extended-face monochromator crystal, *M*, its mosaic spread and the interaction of the wavelength dispersions of *M* and of *c*. The last component contributes significant variation in shape with change in $\theta_c$, or, more generally, in $t = (\tan\theta_c)/(\tan\theta_M)$. The present approach gives a clearer appreciation of the rôles of the various components than occurred in an earlier treatment [Mathieson (1985). *Acta Cryst.* A41, 309-316] and so has heuristic value as an aid in obtaining a proper understanding of the interaction between source/monochromator crystal/specimen crystal and also in estimating experimental parameters for modelling reflections and defining truncation limits. The graphical approach in $\Delta\omega, \Delta 2\theta$ space can assist in the investigation of special features of Bragg reflections.

## Introduction

For the measurement, with neutrons or X-rays, of a set of Bragg reflections from a small single-crystal specimen, one feature is basic in order to establish physically significant estimates of structure factors. The regions in a diffraction space* within which the integrated intensity for each reflection is measured must be exactly equivalent, *i.e.* truncated identically.

The appropriate region for each reflection, or, in general terms, its 'shape', corresponding to this truncation condition, is determined by the components associated with the particular experimental arrangement. Whether one is dealing with the shape in two (or three) dimensions or with the projected shape, *i.e.* profile in one dimension (*e.g.* Mathieson & Stevenson, 1986), one requires to be able to define outer limits (box-shaped or elliptical in 2D, scan range and aperture size, for a given scan mode, in 1D) within which the estimation of integrated intensity is carried out. For the case involving only a source and a small single-crystal specimen, *c*, decisions on these matters are, at least superficially, relatively clear cut [*e.g.* Mathieson (1982, 1984) for 2D; Alexander & Smith (1962) for 1D]. With the incorporation of a monochromator crystal, *M*, and hence the interaction of the dispersions of two crystals (and their probable difference in physical size), the situation becomes more complex. Particularly is this the case for neutrons where there are usually no wavelength-identifying features, such as the $\alpha_{1,2}$ doublet with characteristic X-rays.

In these latter circumstances, one may base decisions concerning the shape of the outer limit figure on purely *ad hoc* procedures without attempting to determine the appropriate component parameters (*e.g.* Spencer & Kossiakoff, 1980; Sjölin & Wlodawer, 1981). However, there are limitations to this approach since, with increasing Bragg angle $\theta_c$ of the specimen crystal, reflections tend to increase in size and also become intrinsically weaker, with the result that outer boundaries are progressively more difficult to ascertain. The alternative is to base decisions concerning shape on a theoretical model. It is, however, essential that the theoretical model should be physically realistic, *and can be identified as such*, and that its predictive capability is authentically effective over the full working range of $\theta_c$.

The earlier approaches to theoretical modelling of neutron reflections involved analytical methods (*e.g.* Willis, 1960; Werner, 1971). The shape for each reflection could, in principle, be calculated using component values estimated from independent experimental measurements. Since all components are treated together in a general formula, it is not easy to recognize how the various physical factors interact or to visualize how the various components contribute to the 'shape', nor conversely how to nominate specific regions of $\theta_c$ which are sensitive in relation to particular component parameters, although Dachs (1978) offers interpretations which, from the present analysis, appear more specific than is warranted. In

* For the intercomparison of Bragg reflections differing in Bragg angle, one should recognize the distinction between $\Delta\omega, \Delta 2\theta$ local angular space and reciprocal space (Mathieson & Stevenson, 1985). 'Diffraction space' is used as a general term encompassing both.

0108-7673/88/061036-07$03.00 

fact, while limited tests have been applied to selected one-dimensional aspects of Bragg reflections (Pantazatos & Werner, 1973; Sequeira, 1974), a full-scale 2D comparison of theoretical distributions with the corresponding experimental equivalents, using this procedure, does not appear to have been attempted and so verification of the overall effectiveness of the analytical approach remains to be established. In addition, the analytical approach generally requires simplifying assumptions concerning the functional form of components to allow its use.

An alternative approach to the derivation of the shapes of Bragg reflections has been taken, independently, by Mathieson (1982) and by Schoenborn (1983). This recognizes that the reflection shape results from convolution of the distributions associated with the various components. This 'diagram' or graphical approach involves recognition of the loci of the various components in $\Delta\omega, \Delta 2\theta^{(0)}$ space, identification of the individual distributions and, where relevant, of their functional change with $\theta_c$. Because there is a relatively direct connection of component loci with reflection shape in $\Delta\omega, \Delta 2\theta^{(s)}$ space, it should be feasible to use a selected sample group of reflections to yield the basic parameters with which the whole set of reflections within the working range of $\theta_c$ can be modelled, without recourse to additional independent (external) measurements.

The current investigation started from a study of the neutron single-crystal measurements by Sequeira (1974), especially those presented in his Fig. 2, to explore the capability of the 'diagram approach' for extracting suitable parameter measures, based on the modelling presented in Mathieson (1985*a*), hereafter referred to as M85. It became evident that investigation in greater detail than that given in M85, which was directed at the case of X-rays, would be of value in clarifying the physical aspects of the roles of the various components. Such information could be of considerable value in applications to real-life examples in neutron diffraction, not merely for structure-factor measurement but also for the closer study of special features in Bragg reflection shapes, for example in relation to Kikuchi (absorption) lines (see Iida & Kohra, 1979; Wilkins, 1983).

## Basic features of the model

To explore the relation of the components and the resultant 'shapes', the following model is envisaged, essential features being given in Fig. 1. The specimen crystal, $c$, is assumed small, effectively a point. The monochromator crystal, $M$, an extended-face planar crystal diffracting essentially in the symmetrical mode, is assumed large relative to $c$ but, initially, small relative to the source, $\sigma$, so that one is concerned essentially only with angles of incidence on $M$. The monochromator crystal is restricted in length, $M_- M_+$. The source is assumed to be relatively distant from $M$. It is assumed that $M$ consists of crystallites all of an exact spacing $d$, and that the central beam from the source, of wavelength $\lambda_0$, incident on the centre of $M$ and reaching $c$, is diffracted from $M$ at a Bragg angle $\theta_M$. To ensure that the basic physical features are properly identified and their effect demonstrated, the complication associated with depth penetration into $M$ is not introduced here. To avoid confusion liable to arise from use of Gaussian distributions for more than one component and so assist in identifying the role of the mosaic spread of $M$ in relation to the 'shape' of the Bragg reflection, the mosaic spread is taken as triangular, the distribution being given by

$$\mu(\Delta) = 1 - |\Delta|/|\Delta_L| \quad \text{for } |\Delta| < |\Delta_L|$$
$$= 0 \qquad\qquad\qquad \text{for } |\Delta| > |\Delta_L|.$$

From each point on $M$, one may visualize an 'acceptor' fan of rays pointing back towards the region of the source. The 'acceptor' fans from the outer illuminated limits of $M$, namely $M_+$ and $M_-$, and from the central point, $M_0$, are shown in Fig. 1. Each ray of a fan is identified in the inserts in the figure with the corresponding value of $\Delta$ which gives rise to the ray and also of the associated differential wavelength, $\Delta\lambda_n$, deviant from $\lambda_0$. The source is assumed to emit all wavelengths within the band transmitted by the system, uniformly in respect of wavelength and emissivity along the vertical axis - so these are identified as square-wave distributions.

Since the angle $\theta_M$ is defined as positive (Allison & Williams, 1930), it is the negative region of $\omega_c$ which will mainly concern us, that which encompasses the so-called 'parallel' configuration. To avoid

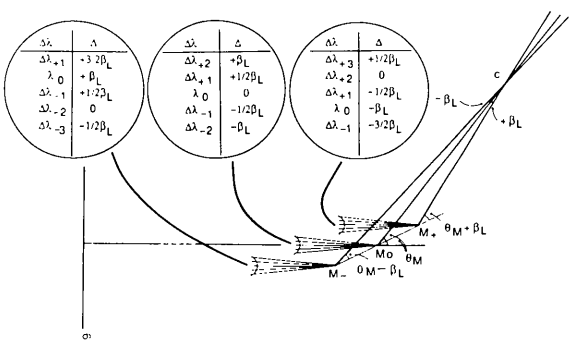


Fig. 1. The arrangement of source, $\sigma$, monochromator crystal, $M$, and specimen crystal, $c$, in the model treated. $M_0$ is the central point of $M$ while $M_-$, $M_+$ are the limit points which subtend the aperture angle $\pm\beta_L$ at $c$. The beams extending from specific points on $M$ back to the source are referred to as 'acceptor fans'. The beams from the source incident on $M_-$, $M_0$, $M_+$ and diffracted to $c$ are identified in the insets with specific values of the mosaic distribution $\Delta$ *and* their corresponding wavelength deviations from $\lambda_0, \Delta\lambda$. Each beam from a point on $M$ going to $c$ has a certain wavelength band composition which changes with location on $M$.

the confusion of increasing negative angles, we will designate the angle $(-)\omega_c$ (see M85).

### Wavelength dispersion in $\Delta\omega, \Delta 2\theta^{(0)}$ space for $\Delta = 0°$

In this section, we deal with the situation for zero mosaic spread, *i.e.* $\Delta = 0$, since this allows us to establish wavelength references corresponding to symmetrical reflection from the surface of $M$ and identify the locus of the source component. Fig. 2 presents the basic features in $\Delta\omega, \Delta 2\theta^{(0)}$ space in relation to diffraction from $c$. The origin $O$ corresponds to the central beam in Fig. 1, incident on and symmetrically diffracted to $c$ from the centre of $M$, $M_0$, its wavelength being $\lambda_0$. $O'$ (at $-\beta_L, -\beta_L$) corresponds to the beam symmetrically diffracted from $M_+$ with a scattering angle $2\theta_M + 2\beta_L$ and of deviant wavelength, $\Delta\lambda_{+2}$, while $O''$ (at $+\beta_L, +\beta_L$) corresponds to the equivalent beam for $M_-$, $2\theta_M - 2\beta_L$, of deviant wavelength, $\Delta\lambda_{-2}$. These define the points $O'$, $O$ and $O''$ for $\theta_c = 0°$ (see Mathieson, 1985*b*). The line $O'OO''$ is at 45° to both $\Delta\omega$ and $\Delta 2\theta^{(0)}$ axes. The loci of $\Delta\lambda_{+2}$ and of $\Delta\lambda_{-2}$ are represented by $Z'_+ O'Z'_-$ and $Z''_- O''Z''_+$ respectively, lines which are parallel to one another at a slope of arctan(1/2) to the $\Delta 2\theta^{(0)}$ axis. For $\theta_c = 0°$, dispersion due to $c$ is zero, so the 'shape' corresponds to the line $O'OO''$. As $\theta_c$ changes from zero to increasing $(-)\omega_c$ values, $\Delta\lambda_{+2}$ moves from $O'$ along $O'Z'_-$ by an amount proportional to $t(=\tan\theta_c/\tan\theta_M)$ and $\Delta\lambda_{-2}$ moves from $O''$ along $O''Z''_-$, also proportional to $t$, $\lambda_0$ remaining stationary at $O$. The locus of the wavelength band, $\Delta\lambda_{+2} - \lambda_0 - \Delta\lambda_{-2}$, therefore corresponds to a straight line, its limits following the lines $Z'_+ O'Z'_-$ and $Z''_- O''Z''_+$ so that it pivots about the origin $O$.

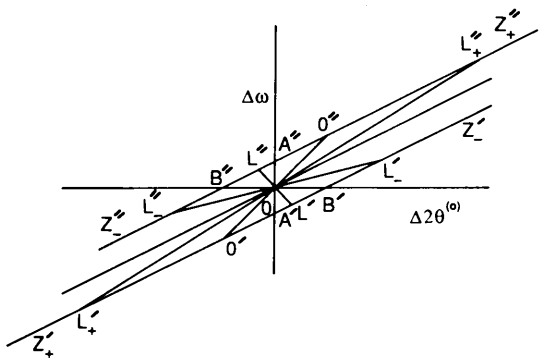


Fig. 2. The variation of wavelength dispersion with $t$ $(=\tan\theta_c/\tan\theta_M)$ in $\Delta\omega, \Delta 2\theta^{(0)}$ space for the case of zero mosaic spread, $\Delta = 0°$. The wavelength band incident on $M_0$ is $\Delta\lambda_{+2} - \lambda_0 - \Delta\lambda_{-2}$, $\lambda_0$ corresponding to the central beam incident on and diffracted from $M_0$ while $\Delta\lambda_{+2}$ and $\Delta\lambda_{-2}$ identify the wavelength deviants from $\lambda_0$ which are diffracted symmetrically from one end, $M_+$, and the other, $M_-$, respectively (see Fig. 1). This defines the points $O'$ and $O''$, the line $O'OO''$ being at 45° to both the $\Delta\omega$ and the $\Delta 2\omega^{(0)}$ axes. $Z'_+ O'Z'_-$ and $Z''_- O''Z''_+$ correspond to the loci of $\Delta\lambda_{+2}$ and $\Delta\lambda_{-2}$ respectively; they lie at a slope of arctan (1/2) to the $+\Delta 2\theta^{(0)}$ axis. As $\theta_c$ changes from zero to increasing $(-)\omega_c$, $\Delta\lambda_{+2}$ moves along $O'Z'_-$, and $\Delta\lambda_{-2}$ moves along $O''Z''_+$, $\lambda_0$ remaining stationary at $O'$ and $O''$. So the locus of the wavelength band, $\Delta\lambda_{+2} - \lambda_0 - \Delta\lambda_{-2}$, corresponds to a straight line, its limits following the lines $Z'_+ O'X'_-$ and $Z''_- O''Z''_+$ so that it pivots around $O$. $L'OL''$ represents one such position of the wavelength band in $\Delta\omega, \Delta 2\theta^{(0)}$ space. The lines $Z'_+ O'Z'_-$ (and $Z''_- O''Z''_+$) are linearly scaled in $t$ (for $\Delta = 0°$). They intersect the $\Delta\omega$ axis at $A'$ (and $A''$) where $t = -0{\cdot}5$ and the $\Delta 2\theta^{(0)}$ axis at $B'$ (and $B''$) where $t = -1{\cdot}0$. The segment $O'Z'_-$ (and $O''Z''_-$) corresponds to the negative region of $t$ which encompasses the 'parallel' arrangement of $c$ and $M$ while $Z'_+ O'$ (and $Z''_+ O''$) corresponds to the positive region of $t$ which encompasses the 'antiparallel' arrangement of $c$ and $M$.

By slight modification of equations (1) and (2) in M85, we obtain

$$(-)\Delta\omega = k'(\beta)[t+1] \qquad (1a)$$

$$(-)\Delta 2\theta^{(0)} = k'(\beta)[2t+1] \qquad (2a)$$

where $t = \tan\theta_c/\tan\theta_M$ and $k'(\beta) = (\Delta\lambda_\beta/\lambda_0)\tan\theta_M$. Sign conventions are based on Allison & Williams (1930) and the terminology follows Mathieson (1983). Relations (1*a*) and (2*a*) ensure that the lines $Z'_+ O'Z'_-$ and $Z''_- O''Z''_+$ are *linearly scaled in t*. As noted above, $O'$ is the reference origin of $Z'_+ O'Z'_-$ and $O''$ of $Z''_- O''Z''_+$ where $t = 0$ ($\theta_c = 0°$). $Z'_+ O'Z'_-$ intersects the $\Delta\omega$ axis at $A'$ and $Z''_- O''Z''_+$ at $A''$ where $t = -0{\cdot}5$ and the $\Delta 2\theta^{(0)}$ axis at $B'$ and $B''$ where $t = -1{\cdot}0$. So the locus of the wavelength band (for $\Delta = 0°$) is $A'OA''$ for $t = -0{\cdot}5$ and $B'OB''$ for $t = -1{\cdot}0$. $L'OL''$ represents a general position of the wavelength band.

The segment $O'Z'_-$ (and $O''Z''_-$) corresponds to the negative region of $t$ which encompasses the 'parallel' arrangement of crystals $c$ and $M$ while the segment $Z'_+ O'$ (and $Z''_+ O''$) corresponds to the positive region of $t$ which encompasses the 'antiparallel' arrangement of $c$ and $M$. The distinction between the magnitude of the dispersion in the two regions is indicated by comparing $L'_- OL''_-$ and $L'_+ OL''_+$ at $t = -1{\cdot}5$ and $+1{\cdot}5$ respectively. In respect of Fig. 2, wavelengths which are positive deviant from $\lambda_0$ are to the right of $O'OO''$ while negative deviant wavelengths are to the left.

To demonstrate more specifically how the $\lambda$ component (for $\Delta = 0°$) changes in magnitude and orientation in $\Delta\omega, \Delta 2\theta^{(0)}$ space, Fig. 3 focuses on the variation in the neighbourhood of the 'parallel' region in 0·25 steps from $t = 0$ to $-1{\cdot}0$ and 0·5 steps to $-2{\cdot}0$.

### Inclusion of the mosaic-spread component of the monochromator crystal

The beams from the source, incident on $M_-$, $M_0$, $M_+$ and diffracted to $c$, correspond to certain specific values of the mosaic spread distribution, $\Delta$, *and* their

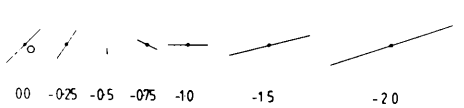


Fig. 3. A more specific demonstration of how the $\lambda$ component (for $\Delta = 0°$) changes in magnitude and orientation in $\Delta\omega, \Delta 2\theta^{(0)}$ space, with particular reference to the 'parallel' region for $t = 0$ to $t = -2{\cdot}0$ in steps of 0·25.

associated wavelength deviation from $\lambda_0$, $\Delta\lambda_n$, as identified in Fig. 1. So each beam from a point on $M$ passing to $c$ has a certain wavelength band composition. This composition changes with position on $M$ and so with $\beta$. These multi-wavelength beams are incident on $c$ and, as $c$ rotates ($\omega$), each component wavelength interacts with $c$ and is dispersed according to its wavelength.

For any given value of $\beta[=\Delta\theta_M(\beta)=(\Delta\lambda_\beta/\lambda_0)\times\tan\theta_M]$, we obtain for any $\Delta\lambda_i$ the relationships

$$\Delta\omega = k'(\beta)[(\Delta\lambda_i/\Delta\lambda_\beta)t+1] \qquad (1b)$$

$$\Delta 2\theta^{(0)} = k'(\beta)[2(\Delta\lambda_i/\Delta\lambda_\beta)t+1]. \qquad (2b)$$

$\Delta\lambda_\beta$ is the fixed value for any $\beta$ when $\Delta=0°$ while $\Delta\lambda_i$ corresponds to any general value within the wavelength band. The magnitude of $\Delta\lambda_i/\Delta\lambda_\beta$, *i.e.* its extent in $\Delta\omega$, $\Delta 2\theta^{(0)}$ space, is dependent on the value of $t$. For each value of $\beta$, (1*b*) and (2*b*) define a line in $\Delta\omega$, $\Delta 2\theta^{(0)}$ space which is the locus of $t$ and lies at a slope of arctan (1/2) to the $+\Delta 2\theta^{(0)}$ axis.

The relationships in (1*b*) and (2*b*) cannot be depicted conveniently in a single diagram but require a series of diagrams to demonstrate the functional dependence on $t$. Fig. 4 depicts this for $t=0$ to $-1{\cdot}0$ in steps of $-0{\cdot}25$ and then to $-2{\cdot}0$ in steps of $-0{\cdot}5$, *i.e.* essentially in the 'parallel' region. For the purposes of demonstration, we assume a largish mosaic spread of $M$ capable of 'filling' the aperture $\pm\beta_L$ at $c$ set by the physical dimensions of $M$. The source is assumed capable of 'filling' all 'acceptor fans' incident on $M$ (see Fig. 1). The triangular mosaic spread is indicated by the dashed lines in Fig. 4.

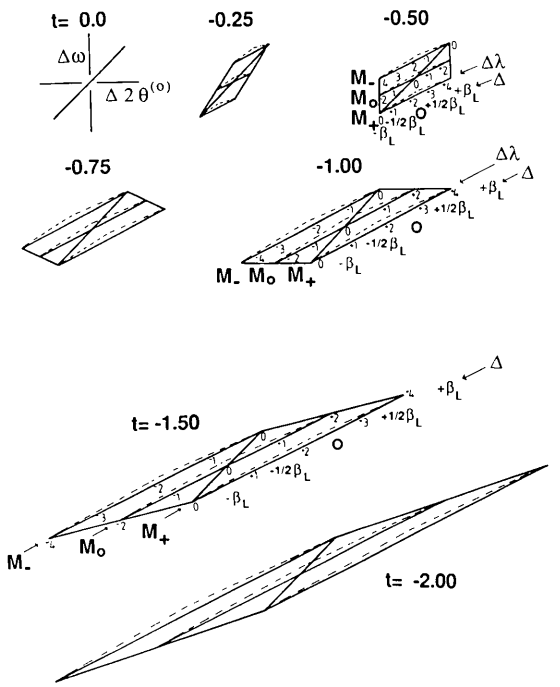


Fig. 4. Demonstration of the variation of the 'shape' of Bragg reflections with change in $t$ in the 'parallel' region from $t=0$ to $t=-2{\cdot}0$. Specific values of $M$, $\Delta\lambda$ and $\Delta$ are identified for $t=-0{\cdot}5$, $-1{\cdot}0$ and $-1{\cdot}5$; their location in the other diagrams can be deduced. In this case, the mosaic spread of $M$ (triangular in distribution) is assumed large enough to 'fill' the aperture $\pm\beta_L$ at $c$ set by the physical dimensions of $M$.

Certain observations on features in Fig. 4 are of interest.

(*a*) From the fixed points, $O'$ and $O''$ (see Mathieson, 1985*b*), lines extend, of length proportional to $t$, both being at a slope arctan (1/2) to the $+\Delta 2\theta^{(0)}$ axis, one from $O'$ going mainly in the positive direction, the other from $O''$ going mainly in the negative direction. These two lines constitute the lower and upper bounds respectively of the 'shape' of the Bragg reflection in respect of the model treated here.

(*b*) The mosaic spread of the monochromator crystal $\mu(\Delta)$ - depicted as a dashed triangular distribution in Fig. 4 (visualized as intensity normal to the plane of the diagram) - extends parallel to these reference lines symmetrically about $\Delta=0°$, the spread being proportional to $t$.

(*c*) The locus through any given wavelength, $\lambda_n$ (say), lies at a slope of 45° to the $\Delta\omega$ and $\Delta 2\theta^{(0)}$ axes.

(*d*) The emissivity distribution, $I(y)$, of $\sigma$ is the distribution along the line of $\Delta=0°$ and therefore with change of $t$ rotates about $O$ as shown in Fig. 3.

(*e*) Except in the special case of $t=-1{\cdot}0$ (the 'parallel' condition), the intensity distribution parallel to $\Delta 2\theta$ at any value of $\Delta\theta$ is *not* a scaled version of that through $\Delta\omega=0°$ (*cf.* Werner, 1971). This difference is less obvious when Gaussian functions are used for the source $\sigma$ and the mosaic distribution $\mu$.

Consider the situation where the mosaic spread of $M$ is very much smaller than that used above but still significantly different from 'zero' mosaic spread. Fig. 5 shows this for the series of $t$ values to indicate how the shape rotates, first contracting 'vertically' and then expanding 'horizontally' with increase in $t$. One may note by inspection of Fig. 5 that, for this situation, the values of the width of the reflection through the peak centre parallel to $\Delta 2\theta$, $\delta_{WS}$,* at $t=-0{\cdot}50$ and at $t=-1{\cdot}0$ can provide first estimates at least of the dimensions of the two components, mosaic spread and the activated length of the monochromator. Note also that, in these circumstances, the width of the 1D profile parallel to $\Delta\omega$, $\sigma_{WS}$ at $t=-1{\cdot}0$ is essentially the same size as $\delta_{WS}$ at $t=-0{\cdot}50$. Here the relative angular sizes of $\mu$ to the aperture $\beta_L$ as judged at $t=-0{\cdot}50$ and $-1{\cdot}0$ is 0·20 to 0·9. If, for illustration, one uses Gaussian distributions for $\mu$ and $\beta$ with

* To avoid confusion with symbols ($\mu$, $\sigma$, $\lambda$, $\delta$) used previously (*e.g.* Mathieson & Stevenson, 1986), the symbols, $\delta$, $\sigma$, used by Werner (1971) and Sequeira (1974) for the width parallel to $\Delta 2\theta$ of the Bragg reflection and the 1D 'counter' profile width respectively are subscripted WS.

such relative half-widths to calculate the resultant 2D Gaussian shape and derive theoretical estimates of $\delta_{WS}$ and $\sigma_{WS}$ over the range of $t$, there is close accord with the *theoretical estimates* by Sequeira using Werner's analytical approach in Figs. 2 and 3 of Sequeira (1974). Note that we are comparing the *theoretical curve* derived from Sequeira with the *theoretical curve* derived from the present approach. One may deduce from the closeness of fit between the two theoretical curves that, in Sequeira's analytical modelling, only these two components were of significant magnitude; all others were of minor consequence.

So far, we have assumed a source of radiation which can 'fill' the acceptance capability of the monochromator crystal. Let us now revert to the large mosaic spread as in Fig. 3 but suppose the source truncated in size so that only those beams $\beta_L/2$ on either side of parallelism to the central beam (see Fig. 1) can excite diffraction. This would mean (see Fig. 1) that $M_+$ is restricted to the wavelength range $\lambda_0$ to $\Delta\lambda_{+2}$, $M_0$ to $\Delta\lambda_+$ through $\lambda_0$ to $\Delta\lambda_-$ and $M_-$ to $\Delta\lambda_{-2}$ to $\lambda_0$. With this combination, a rather different series of shapes results (Fig. 6) from that in Fig. 5.

Different selections of restrictions on the source would lead to other sequences of shapes (*e.g.* Stevenson, 1988).

For illustration of the 'diagram' approach, we can invoke specific severe restrictions of interest in terms of the physical situation. Thus, if we imagine a restriction to *only* those beams parallel to the central beam, the resultant series of shapes would be such that the 'parallel' condition occurs at $t = -2{\cdot}0$ [see (1*b*) and (2*b*), which correspond to the condition $\Delta = 0°$] and not at $t = -1{\cdot}0$. In that case, the 'shapes' are lines (*cf.* Fig. 3) because they correspond to a point source, in this case at infinity. So it is evident that the 'minimum condition can occur at points other than $t = -1$ (*cf.* Willis, 1960; Mathieson, 1988).

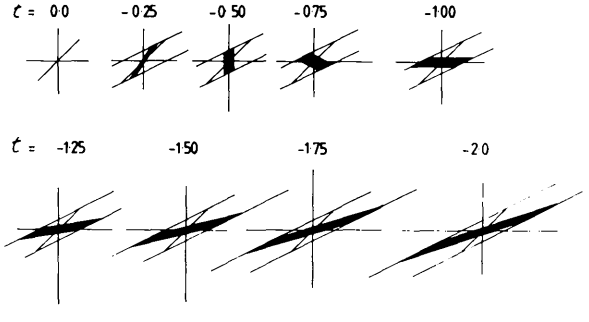


Fig. 5. Demonstration of the variation of shape where the mosaic distribution is smaller than that in Fig. 4. One may note that the width ($= \delta_{WS}$) of the reflection at $t = -0{\cdot}50$ is the same as the height ($= \sigma_{WS}$) at $t = -1{\cdot}0$, and also that the slice width at $t = -1{\cdot}0$ is a measure of the size of the effective source. Hence, in such a case where the mosaic spread of $M$ and the 'size' of the effective source are the main components, one can derive essential parameters to model all reflections from experimental estimates of reflections at $t = -0{\cdot}50$ and $-1{\cdot}0$.

If one considers the case where the source/monochromator and monochromator/specimen distances are equal, then the result would correspond to the central wavelength being $\lambda_0$ with a spread of deviant wavelengths on either side. Under these circumstances, for profile measurement, an $\omega/\theta$ ($s = 1$) scan mode would be appropriate, with the detector aperture adjusted according to the value of $t$.

Combination of restrictions on the source size with the influence of the mosaic spread of $M$ will correspond to the merger of (say) the diffracting capability of Fig. 5 with the 'window' of Fig. 6. For this combination, the results are shown in Fig. 7.

If the source cannot be visualized as effectively at infinity but is at some more realistic distance then the wavelength band associated with $M_+$ and $M_-$ will be displaced, *e.g.* for $M_+$ from $\Delta\lambda_{+2} - \lambda_0$ to (say) $\Delta\lambda_{+1} - \Delta\lambda_{-1}$ with a corresponding change for $M_-$ of $\Delta\lambda_{-2} - \lambda_0$ to $\Delta\lambda_{-1} - \Delta\lambda_{+1}$. This would cut further into the shapes in Fig. 7 and truncate the areas further (see also Stevenson, 1988).

## Discussion

The present work constitutes a re-examination of the interactions of the various components of the system source/monochromator crystal/specimen crystal which is based on the very minimum of assumptions

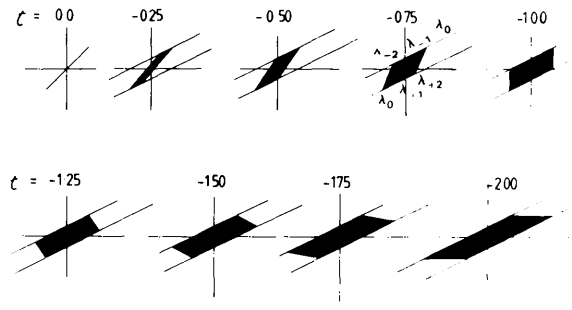


Fig. 6. Demonstration of the variation of shape where the limiting feature is the source size. Here the source is truncated so that only those beams $\pm\beta_L/2$ on either side of parallelism to the central beam can excite diffraction. In the case shown, the mosaic spread of $M$ is assumed large - as in Fig. 4.

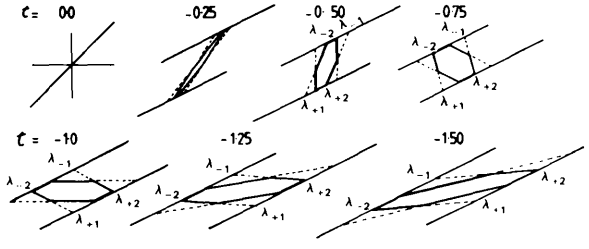


Fig. 7. Combination of the diffracting capability associated with Fig. 5 with the source 'window' illustrated in Fig. 6 leads to the shapes in this figure.

and is more detailed than that given in M85. The contributions from each component distribution are identified in $\Delta\omega, \Delta 2\theta^{(0)}$ space and so the shape, and the intensity distribution, appropriate to film observation or to linear position-sensitive detectors (without conversion to reciprocal space) can be deduced from a knowledge of the individual distributions. Conversely, from a survey of selected reflections spanning the range of $t$, one can deduce experimental parameters for the individual distributions, particularly from reflections at special values of $t$, such as $t = -0{\cdot}50$ and $-1{\cdot}0$.

Comparison of the shapes derived from the theoretical model treated in the present paper with those presented in M85 shows changes of emphasis. Certain features are common. Thus, the locus in $\Delta\omega, \Delta 2\theta^{(0)}$ space for any given wavelength component $\lambda_n$ lies at 45° to both $\Delta\omega$ and $\Delta 2\theta^{(0)}$ axes. The intensity distribution along the locus, which was designated $\sigma/\mu_M$ in M85, corresponds in fact to a secondary manifestation of the mosaic distribution of the monochromator crystal. The primary manifestation of the mosaic spread at a given point on $M$ has a locus at a slope of arctan (1/2) to the $+\Delta 2\theta^{(0)}$ axis (see Fig. 4). The distribution along the locus for $\lambda_n$ involves the change in the mosaic distribution along $M$. If the mosaic distribution is the same at all points of $M$ then the distribution along $\lambda_n$ is the same as the primary manifestation, *i.e.* triangular, as assumed here.

The primary manifestation of the source distribution corresponds to the distribution along the locus of $\Delta = 0°$ which is also the locus of $\lambda$ from $\Delta\lambda_{-2}$ to $\Delta\lambda_{+2}$. In the earlier model in M85, this was referred to as the locus of $\lambda$; that nomination arose because $\Delta = 0°$ corresponded to the reference state of zero mosaic spread and thus focused attention on the variation in respect of $\lambda$.

When one examines the situation where the mosaic spread is fairly wide, as in Fig. 4, focusing (say) on $\Delta\lambda_{-1}$ and $\Delta\lambda_{+1}$, then one observes that these components are related symmetrically about the origin. Thus, for example, for the case where $t = -1{\cdot}0$ in Fig. 4, the intensity of $\Delta\lambda_{-1}$ runs from zero (in the region of negative $\Delta\omega$) to maximum intensity and down to half maximum (in the region of positive $\Delta\omega$). By contrast, the intensity of $\Delta\lambda_{+1}$ starts from half maximum (in the region of negagive $\Delta\omega$), goes to maximum intensity and down to zero (in the region of positive $\Delta\omega$). In the earlier model in M85, the distributions would have been interpreted as identical.

By inspection of the various diagrams in Fig. 4, one can see that the comparative distributions for $\Delta\lambda_{-1}$ and $\Delta\lambda_{+1}$ depend on $t$ *and* on the magnitude of the separation of $\Delta\lambda_{-1}$ and $\Delta\lambda_{+1}$.

The feature which is distinguished in this analysis is the continual and progressive variation of the band of wavelengths which is diffracted as the specimen crystal rotates in $\Delta\omega$ through the Bragg reflection.

While the box shapes of Bragg reflections deduced in the present work can, depending on the size of the experimental parameters, differ from those deduced by the approach taken in M85, the differences are less evident when the distribution functions are rounded, *e.g.* Gaussians. However, for accuracy of measurement of integrated intensity which depends on proper truncation or for the explicit examination of individual reflections in detail (*e.g.* Iida & Kohra, 1979; Wilkins, 1983) it is advisable to be able to identify how the various components contribute to specific parts of the reflection.

In this text, no mention has been made of the mosaic spread of the specimen crystal. The locus of this component lies parallel to the $\Delta\omega$ axis in $\Delta\omega, \Delta 2\theta^{(0)}$ space and is therefore treated as in the non-monochromator case (*e.g.* Mathieson, 1982).

Discussion of the shape of Bragg reflections has been restricted to $\Delta\omega, \Delta 2\theta^{(0)}$. When other scan modes ($s \neq 0$) are invoked, one can readily deduce how the shape changes. See Fig. 8 for the case of $s = 2$ (which refers to axes $\Delta\omega$ and $\Delta 2\theta^{(2)}$) and Mathieson (1985*c*), which was, however, based on the earlier modelling in M85. As is evident in this case, for profile measurement, a fixed aperture in front of the detector is appropriate for all settings of $\theta_c$.

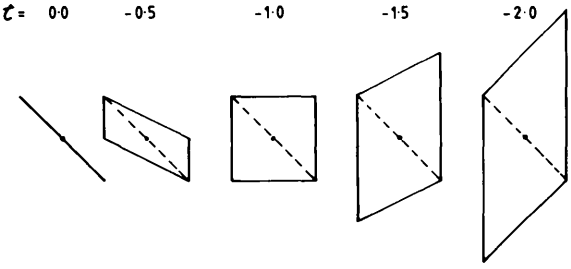


Fig. 8. In the case of the $\omega/2\theta$ scan mode, *i.e.* $s = 2$, the changes in shape in $\Delta\omega, \Delta 2\theta^{(2)}$ space are shown for $t = 0$ to $-2{\cdot}0$ in steps of $-0{\cdot}50$.

I would like to express my appreciation of valuable discussions with Dr A. W. Stevenson who has developed an alternative but related approach to deducing the 'shapes' of Bragg reflections, one which is more suited for computer applications. He intends to treat this elsewhere.

## References

ALEXANDER, L. E. & SMITH, G. S. (1962). *Acta Cryst.* **15**, 983-1004.

ALLISON, S. K. & WILLIAMS, J. A. (1930). *Phys. Rev.* **35**, 149-154.

DACHS, H. (1978). *Principles of Neutron Diffraction.* In *Topics in Current Physics*, edited by H. DACHS, pp. 1-40. Berlin: Springer.

IIDA, A. & KOHRA, K. (1979). *Phys. Status Solidi A*, **51**, 533-542.

MATHIESON, A. McL. (1982). *Acta Cryst.* **A38**, 378-387.

MATHIESON, A. McL. (1983). *J. Appl. Cryst.* **16**, 257-258.

MATHIESON, A. McL. (1984). *Acta Cryst.* **A40**, 355-363.

MATHIESON, A. McL. (1985*a*). *Acta Cryst.* **A41**, 309-316.

MATHIESON, A. McL. (1985*b*). *Acta Cryst.* A**41**, 603-605.
MATHIESON, A. McL. (1985*c*). *J. Appl. Cryst.* **18**, 506-508.
MATHIESON, A. McL. (1988). *Acta Cryst.* A**44**, 239-244.
MATHIESON, A. McL. & STEVENSON, A. W. (1985). *Acta Cryst.* A**41**, 290-296.
MATHIESON, A. McL. & STEVENSON, A. W. (1986). *Acta Cryst.* A**42**, 435-441.
PANTAZATOS, P. & WERNER, S. A. (1973). *Acta Cryst.* A**29**, 557-558.
SCHOENBORN, B. P. (1983). *Acta Cryst.* A**39**, 315-321.
SEQUEIRA, A. (1974). *Acta Cryst.* A**30**, 839-843.
SJÖLIN, L. & WLODAWER, A. (1981). *Acta Cryst.* A**37**, 594-604.
SPENCER, S. A. & KOSSIAKOFF, A. A. (1980). *J. Appl. Cryst.* **13**, 563-571.
STEVENSON, A. W. (1988). *Acta Cryst.* A. In the press.
WERNER, S. A. (1971). *Acta Cryst.* A**27**, 665-669.
WILKINS, S. W. (1983). *Phys. Rev. Lett.* **50**, 1862-1865.
WILLIS, B. T. M. (1960). *Acta Cryst.* **13**, 763-766.

*Acta Cryst.* (1988). A**44**, 1042-1044

# Bethe's Correction Method for Dynamical Calculation of Reflection High-Energy Electron Diffraction Intensities from General Surfaces

BY AYAHIKO ICHIMIYA

*Department of Applied Physics, School of Engineering, Nagoya University, Chikusa-ku, Nagoya* 464-01, *Japan*

(*Received* 22 *February* 1988; *accepted* 8 *June* 1988)

## Abstract

The correction method for weak diffraction of Bethe [*Ann. Phys.* (*Leipzig*) (1928), **87**, 55-129] is applied to dynamical calculation of reflection high-energy electron diffraction (RHEED) intensities from general surfaces based on a multi-slice method. For high-step-density surfaces, it is shown that the corrected surface potential (Bethe potential) depends on the incident direction of electrons for step directions. Furthermore it is shown that the Bethe potential is approximately proportional to the coverage of adsorbed atoms or of terraces of high-step-density surfaces. For the RHEED intensity from stepped surfaces, the intensity oscillation during molecular beam epitaxial growth is discussed. An appropriate calculational formula for reconstructed surfaces is also obtained.

## 1. Introduction

Practical methods of reflection high-energy electron diffraction (RHEED) intensity calculation were proposed by several theoretical studies (Masud & Pendry, 1976; Maksym & Beeby, 1981; Ichimiya, 1983; Peng & Cowley, 1986). These methods are appropriate to perfect crystal surfaces, but most of the methods are not available for imperfect surfaces. The first theoretical formalism for imperfect surfaces was presented with a perturbation method by Beeby (1979). Peng & Cowley (1986) proposed a new method for calculating RHEED intensities which would allow the calculation of intensities from imperfect surfaces. Electron diffraction intensity distributions from imperfect surfaces were interpreted using kinematic diffraction theory by several authors (Matysik, 1974; Henzler, 1977; Holloway & Beeby, 1978; Holloway, 1979; Van Hove, Lent, Pukite & Cohen, 1983; Lent & Cohen, 1984; Pimbly & Lu, 1985; Pukite, Lent & Cohen, 1985). Recently some theoretical approaches were proposed to interpret RHEED intensity oscillations (Van Hove, Lent, Pukite & Cohen, 1983; Kawamura, Maksym & Iijima, 1984; Kawamura & Maksym, 1985; Ichimiya, 1987). In a previous paper (Ichimiya, 1987) RHEED intensities from a surface with low step densities were obtained analytically from Kirchhoff's diffraction theory. From the calculations it was shown that integrated intensities of RHEED scarcely depend on the step distributions and terrace coverage, but the intensities on reciprocal rods depend sensitively on these factors. Kawamura & Maksym (1985) have shown that the oscillation property of RHEED intensities during molecular beam epitaxial (MBE) growth depends on crystal orientation and the step directions for the incident beam because of dynamic diffraction effects. In their calculation dynamic diffraction as high density and periodic distribution of steps was taken into consideration.

In the present work Bethe's correction method (Bethe, 1928; Ichikawa & Hayakawa, 1977) for weak beams in the dynamical theory of electron diffraction was applied to calculation of RHEED intensities from general surfaces such as stepped, reconstructed, distorted or adsorbed surfaces based on the multi-slice method (Ichimiya, 1983).

## 2. Bethe's correction for general surfaces

According to the multi-slice method of RHEED dynamical theory (Ichimiya, 1983), the Schrödinger equation at the $j$th slice parallel to the surface is expressed by a two-dimensional (2D) position vector $\mathbf{r}$ and a 2D wave vector $\mathbf{k}_0$, which are parallel to the

0108-7673/88/061042-03$03.00 